



Article

Exploring Bifurcation in the Compartmental Mathematical Model of COVID-19 Transmission

Olena Kiseleva ¹, Sergiy Yakovlev ² , Dmytro Chumachenko ^{3,4,*}  and Oleksandr Kuzenkov ¹

¹ Faculty of Applied Mathematics, Oles Honchar Dnipro National University, 49000 Dnipro, Ukraine; kiseleva47@ukr.net (O.K.); kuzenkov1986@gmail.com (O.K.)

² Institute of Mathematics, Lodz University of Technology, 90-924 Lodz, Poland; svsyak7@gmail.com

³ Department of Mathematical Modeling and Artificial Intelligence, National Aerospace University "Kharkiv Aviation Institute", 61070 Kharkiv, Ukraine

⁴ Ubiquitous Health Technology Lab, University of Waterloo, Waterloo, ON N2L 3G5, Canada

* Correspondence: dichumachenko@gmail.com

Abstract: This study proposes and theoretically substantiates a unique mathematical model for predicting the spread of infectious diseases using the example of COVID-19. The model is described by a special system of autonomous differential equations, which has scientific novelty for cases of complex dynamics of disease transmission. The adequacy of the model is confirmed by testing on the example of the spread of COVID-19 in one of the largest regions of Ukraine, both in terms of population and area. The practical novelty emerges through its versatile application in real-world contexts, guiding organizational decisions and public health responses. The model's capacity to facilitate system functioning evaluation and identify significant parameters underlines its potential for proactive management and effective response in the evolving landscape of infectious diseases.

Keywords: epidemic process; COVID-19; compartmental model; nonlinear analysis



Citation: Kiseleva, O.; Yakovlev, S.; Chumachenko, D.; Kuzenkov, O. Exploring Bifurcation in the Compartmental Mathematical Model of COVID-19 Transmission. *Computation* **2024**, *12*, 186. <https://doi.org/10.3390/computation12090186>

Academic Editor: Simone Brogi

Received: 12 July 2024

Revised: 22 August 2024

Accepted: 4 September 2024

Published: 11 September 2024



Copyright: © 2024 by the authors. Licensee MDPI, Basel, Switzerland. This article is an open access article distributed under the terms and conditions of the Creative Commons Attribution (CC BY) license (<https://creativecommons.org/licenses/by/4.0/>).

1. Introduction

At the end of 2019, the spread of the SARS-CoV-2 virus led to the outbreak of the COVID-19 epidemic in China. The spread of infection among the population of many countries was so massive that, in January 2020, the World Health Organization identified the outbreak as a public health emergency of international importance [1]. In March 2020, the situation was called a pandemic.

The period of development of the epidemic from a few infected to tens, and in some cases up to hundreds, was measured in weeks and—in some countries—in a few days. Each of the countries that recognized the COVID-19 epidemic was in different conditions (the number of infected people, the state of the healthcare system, the number of equipped infectious disease hospitals, the availability of the necessary medical equipment, the availability of qualified medical personnel, legislation regulating the possibility of introducing restrictive measures, etc.), which undoubtedly influenced the course of epidemics in each country. The rapid development of the pandemic has shown that not always do a well-established economy and a regulated legislative framework make it possible to respond quickly to the challenges of such an emergency as the COVID-19 pandemic turned out to be.

Today, it is evident that organizational methods of combating the spread of COVID-19 are not inferior to medical ones in terms of effectiveness [2]. After the rapid growth in the number of infected people in densely populated cities and their regions, the lack in some countries of the necessary amount of equipment for the care of infected patients, and the refusal of some patients with severe and moderate morbidity of hospitalization, it is essential to predict the number of infected people by some sufficient number to accept the necessary needs, measures, period, and assessment of the qualitative stages of the

development of epidemics in certain territories [3]. The purpose of the mathematical modeling of the spread of COVID-19 is to assess the speed, timing, and stages of its spread, and the effectiveness of specific measures to combat this infection [4]. Each set of measures (closing shops, catering facilities, government agencies, entertainment centers, educational institutions, restricting public transport, etc.) has significant social, production, and economic consequences. Their balanced application makes it possible to combat the spread of the infection, effectively reducing the negative impact of these consequences.

The aim of the paper is to develop new approaches to describing dynamic processes in complex processes and systems, mathematical models for predicting the spread of infectious diseases, and approaches to identifying the parameters of such models, determining the most significant factors influencing the system and methods for managing such systems to achieve their desired state or quality changes in their dynamics.

The promising contribution of this study is two stage. Firstly, a new mathematical model of the dynamics of infectious diseases and approaches to the qualitative study of such a model, analysis of the analytical conditions for qualitative changes in the system (bifurcations), and approaches to the applied interpretation of the results obtained was developed. This allows not only to evaluate the qualitative modes of functioning, but also the methods and results system management. Secondly, the proposed approaches and a mathematical model to predict the dynamics of the spread of an infectious disease, using the example of COVID-19, can be applied to simulate epidemic process dynamics in selected territories. A retrospective analysis showed the high accuracy of the model of the adequacy of recommendations for managing it and allows not only an up-to-date forecast of the state of the system to be obtained, but also recommendations for managing it to change the qualitative modes of operation to be developed.

The further structure of the paper is the following: Section 2, Background, provides an overview of epidemic modeling and the state of current research in COVID-19 simulation with a compartmental approach. Section 3, Materials and Methods, describes the proposed compartmental model of the COVID-19 epidemic process. Section 4, Results, provides a qualitative analysis of the bifurcation properties of a mathematical model. Section 5, Case Study, describes the results and analysis of a numerical experiment of COVID-19 simulation in the Dnipropetrovsk and Kharkiv regions (Ukraine). The Conclusion describes the outcomes of the research.

2. Background

To date, there are a sufficient number of mathematical models for assessing the rate of spread of COVID-19, and each of these models, as a rule, is focused on a particular region (country, region, city, etc.) [5]. Each of these regions differs significantly from the others in the age composition of the population, chronic diseases characteristic of a particular region, social activity of different ages, etc.

Each of these factors does not significantly affect the curve of growth in the number of infected. However, since such a curve is usually exponential, the numerical indicators vary significantly over a sufficient period. An example is Italy, where older people are characterized by high social activity [6]. This situation significantly affected the number of infections among the elderly population and, as a result, the loading of hospitals with “severe” patients and the collapse of the healthcare system in Italy.

Since the total number of infected people in the world today is measured in millions, there is relatively reliable information about the course of the epidemic in certain territories [7]. At the same time, even experienced specialists (epidemiologists) can only describe the course of the disease, but the “physics” of the infection and its effect on the body cannot be described in most cases.

Most specialists use SIR models and extended versions to model the process of infection spread [8]. In most countries, there are no reliable data on the number of infected and dead; the error for the SIR model leads to a rapid accumulation of errors and, consequently, false simulation results. In addition, the SIR model considers only three fundamental

indicators, i.e., it cannot foresee the impact on the system of restrictive measures, and many of them have been invented to date. The actual statement of the course of the spread of the infection is not very informative, and a set of measures is desirable for at least a numerical slowdown in the development of the epidemic or qualitative changes in its course.

To build the mathematical model proposed in work, we took as a basis models that not only adequately, from our point of view, describe the dynamics of infectious diseases but also proved their adequacy and reliability in practice.

One of the founders of the mathematical modeling of epidemics can be considered the American researcher Ross, who first developed models for the migration of infection carriers in 1905 [9], and in 1908–1910 [10,11] proposed a model for the spread of the infection itself. The results obtained by Ross were partly the basis of McDonald's studies [12], which made it already possible to build a model of the spread of infection in the middle of the 20th century, taking into account the entomological and demographic characteristics of the population.

These models were further developed several decades later in the works of Hoppens in 1974, in which a new epidemic model was published that takes into account the age structure of the population [13], and a class of differential systems [14] was proposed that can be used to describe the dynamics of the spread of infection.

Also, the models proposed by Ross were developed in the works of Bailey in the 1990s. Bailey succeeded in extending the Ross model and presenting a model for spreading infection through the SEIR and SEI models. After Bailey's publication, the development of the SEIR and SEI models was put to work by Newton and Reuter, whose research focused on the spread of dengue fever. Other qualitative results of the study of the SEIR and SEI models were obtained in [15,16]. In [17], the authors divided the human population into a finite number of ages. The author determined the base reproductive disease number for the SEIR task of the age-dependent system.

The global COVID-19 pandemic has intensified research on developing mathematical models for modeling infectious diseases.

Paper [18] presents a comprehensive exploration of the time-varying transmission dynamics of the COVID-19 epidemic in Korea using a Susceptible–Exposed–Infectious–Recovered–Dead (SEIR(D)) model. It argues that understanding the epidemic's multi-stage development leads to a more nuanced appreciation of the infection's changing patterns, heavily influenced by non-pharmaceutical interventions (NPIs) implemented by the public health authority. By applying the SEIR(D) model to three distinct stages of the pandemic, using a dataset spanning from 18 February 2020 to 8 February 2021, the research uncovers the unique transmission patterns of SARS-CoV-2 in each phase. The study underscores the limitations of using a generic SIR compartment model across the entire epidemic period, advocating instead for a context-sensitive application of the SEIR(D) model that acknowledges the multi-wave nature of the pandemic and the varying effectiveness of NPIs over time.

The research in [19] offered predictive analyses regarding the spread of COVID-19 and its significant impact on hospital care in Lombardy and Emilia-Romagna, the two regions of Italy most heavily affected by the epidemic. Utilizing a Susceptible–Exposed–Infectious–Recovered deterministic model—augmented by an additional compartment L to account for the isolated infected population who do not require hospital care—the researchers analyzed the implications of varying conditions of social distancing. The findings indicated that Lombardy would benefit from extending restrictive containment measures until early July to prevent a rebound in hospitalizations. Conversely, in Emilia-Romagna, it was proposed that a higher contact rate could maintain the number of hospitalized cases at a manageable level. Ultimately, this research underscores the importance of region-specific forecasts under differing scenarios, which can inform and optimize containment strategies during the epidemic.

The study by A. Bhalraj and A. Azmi [20] offers predictive insights into the outbreak of COVID-19 using the SEIR model, preferred over the SIR model due to the significant

contribution of asymptomatic or mildly symptomatic individuals to the transmission of the disease. The paper provides a model encapsulating the transmission dynamics of COVID-19 amidst implementing three key intervention measures: preventive measures, active case finding, and hospitalization interventions. It offers an evolving depiction of the disease spread within a population under these control strategies aimed at eradicating it. Simulating the COVID-19 model with various levels of intervention effectiveness, the study observes and analyzes divergent outcomes for infectious individuals. The simulation results suggest that more rigorous and stringent public health interventions could curtail the spread of COVID-19. The study underscores the crucial practical significance of early prevention, detection, and treatment in the battle against COVID-19.

Paper [21] presents a novel SQEIHDR mathematical model designed to predict the transmission dynamics of COVID-19 in India, an extension of the foundational SEIR model with the incorporation of additional compartments representing self-quarantine (Q), isolation (H), and deceased (D) individuals. By encompassing these additional elements, the model aims to provide a more accurate depiction of the COVID-19 outbreak in India and potential strategies to inhibit transmission increase. Spanning ten phases with varying COVID-19 preparedness and response plans, the model's simulation demonstrates significant fluctuations in the infection curve, contingent on the changes in the self-quarantine compartment (Q). The results emphasize the effectiveness of the implemented and proposed preparedness and response strategies, highlighting the critical role of the rate of self-quarantine (Q)—a factor influenced by general awareness, social distancing, and food availability—in precipitating a downturn in the outbreak.

The authors of [22] introduce the SEPIR model—an enhancement of the classic SEIR continuous simulation compartment model—introducing an additional presymptomatic infectious compartment to capture a critical aspect of COVID-19's transmission dynamics. While both models can be fitted to actual data via estimable parameters, the SEPIR model's inclusion of the presymptomatic stage allows for a more comprehensive representation of COVID-19. The study primarily explores fitting the SEPIR model to a first wave of COVID-19, acknowledging that both the SEIR and SEPIR models operate under the assumption of a homogeneous mixing population with fixed parameters and do not account for dynamically varying control strategies. To extend these models beyond a single wave of the epidemic, the study proposes the implementation of time-dependent parameters. Furthermore, the paper illustrates how reproduction numbers can be calculated to evaluate the long-term overall outcome of an epidemic.

Paper [23] focuses on applying the SIR model to understanding the trajectory of the COVID-19 pandemic and devising potential intervention measures. The SIR model, renowned for its efficacy in epidemic analysis, is utilized in this paper to elucidate the patterns of COVID-19 spread and the future trends of the disease. The researchers examine the critical parameters within the SIR model, particularly the contact and reproduction ratios, identified as critical factors with the potential to mitigate COVID-19's consequences. In light of their analysis, the research advocates for specific anti-COVID-19 measures, such as mask-wearing, hand hygiene, social distancing, and staying home where possible. The study underscores the pivotal role of the SIR model in informing public health emergencies and strategizing appropriate interventions.

H.M. Youssef et al. [24] presents a modified SEIR model tailored explicitly for predicting the spread of COVID-19, demonstrating its effectiveness using actual data from Saudi Arabia. The modified SEIR model offers a novel perspective for evaluating and managing the COVID-19 epidemic, with the dynamic analysis including calculations of the reproduction number and extensive stability analyses. Using Jacobian's method of linearization, the paper discusses the solution domain and equilibrium states for the proposed model. The conditions and uniqueness of the equilibrium are established, followed by a stability analysis of disease-free equilibrium states. Further, a sensitivity analysis of the reproduction number concerning its internal parameters is conducted, and global stability is demonstrated using Lyapunov's Stability theorem. Comparative numerical

validation of the proposed model, juxtaposed against actual data, shows the model's effectiveness in predicting the spread of COVID-19 in Saudi Arabia. The study ultimately introduces an optimal protocol designed to curtail the spread of COVID-19 within the Saudi population rapidly.

Paper [25] introduces the SEIAQRDT model, a refined mathematical model devised to address the inadequacies of previous epidemiological models (such as SIR, SEIR, SIRD, and SEIRD) in accurately forecasting the spread of COVID-19. This novel model incorporates infected individuals based on symptom presence, enhancing the accuracy of predicting case numbers and developing more effective control strategies. The model comprises eight compartments: Susceptible (S), Exposed (E), Infected (I), Asymptomatic (A), Quarantined (Q), Recovered (R), Deaths (D), and Insusceptible (T). The paper applies this model to predict pandemic outcomes in India and its most severely affected states. It compares the SEIAQRDT estimations with those of the SIRD, SEIR, and LSTM models. Verification of the proposed model's accuracy is performed using the relative error square analysis on real datasets, with the simulation results affirming the model's efficacy. The findings could assist the government and individuals in devising more informed pandemic response strategies.

Study [26] presents a novel nonlinear SIR epidemic model designed to examine the spread of COVID-19, emphasizing the influence of public policy measures, such as government-induced social distancing, in curbing the pandemic. By tailoring parameters to specific countries like Germany, Spain, Italy, France, Algeria, and Morocco, the model is fitted to real-world data, enabling an assessment of the effectiveness of government measures in each country vis-à-vis the evolution of the pandemic. The utility of this model lies in its potential to serve as an efficient instrument in forecasting disease spread, thereby assisting in the formulation and implementation of future public health policies and strategies to control the pandemic.

Paper [27] employs the SIR and SIR-D models, prominent epidemiological tools that categorize individuals into specific groups or compartments, to simulate the spread of the COVID-19 pandemic in Indonesia. Three scenarios were simulated: a condition without vaccination, a condition with vaccination, and a scenario incorporating vaccination but lacking stringent health protocols. The models' simulations indicated that, while the vaccination process can mitigate the spread of COVID-19, its impact is less profound due to suboptimal and non-comprehensive vaccination practices. However, if vaccinations are conducted without stringent health protocols, the rapid spread of the virus and a subsequent second wave is likely. Thus, maintaining adherence to health protocols is underscored even amidst the vaccination process. With Mean Absolute Percentage Error accuracy levels of 0.41198 and 0.01712 for the SIR and SIR-D models, respectively, these epidemiological models provide a valuable tool for visualizing and understanding the dynamics of COVID-19 transmission.

Paper [28] utilizes the SEIR model, a type of compartmental model, to simulate and forecast the trajectory of the COVID-19 pandemic within the six countries that reported the most cases by the end of 2020—the United States, Russia, the United Kingdom, France, Brazil, and India. Applying the fourth-order Runge–Kutta method to solve the SEIR model equations, the study draws on confirmed case data up until 29 December 2020, to derive parameters for the model. The analysis allows for extracting coefficients for the Exposed, Infected, Recovered, and mortality rate parameters in the SEIR model, thus providing a nuanced understanding of disease progression in these countries. The study predicts the infection peaks for these countries to occur in the first half of 2021, with the average basic reproduction number of SARS-CoV-2 calculated at 2.1460. The findings underscore the utility of the SEIR model in facilitating an accurate forecast of infectious disease spread, which can inform effective public health responses.

Table 1 presents the current research analysis of the COVID-19 compartmental models.

Table 1. Current research analysis of COVID-19 compartmental models.

Paper	Task	Compartments	Findings
H.Y. Shin [18]	To analyze the time-varying transmission dynamics of the COVID-19 epidemic in Korea throughout its multiple stages of development	Susceptible, Exposed, Infected, Recovered, Dead	The transmission dynamics of the COVID-19 vary over time, primarily depending on the relative effectiveness of the government’s non-pharmaceutical interventions.
C. Reno, et al. [19]	To forecast the spread of the infection and its burden on hospitalizations under different conditions of social distancing in Lombardy and Emilia-Romagna (Italy)	Susceptible, Quarantined Susceptible, Exposed, Quarantined Exposed, Infectious with Symptoms, Isolated Infectious, Infectious without Symptoms, Hospitalized, Recovered	Analyzing the burden of hospitalizations under different conditions of social distancing allows foreseeing the impact of the coronavirus pandemic on health services.
A. Bhalraj and A. Azmi [20]	To implement SEIR mathematical model to forecast the future of COVID-19 in terms of the number of days it will take to reach the peak and also to contain the outbreak	Susceptible, Exposed, Infected, Recovered	In order to curb COVID-19 outbreak, combined interventions are crucial and, hence, these combined interventions include all kind of preventive measures, active case finding, and hospitalization such as enforcement of wearing masks, using hand sanitizer regularly, maintaining social distancing, in-home quarantine, minimizing outdoor activities, obeying lockdown and movement control order, conducting active case detection, and providing essential medical equipment for infected individuals as well as personal protective equipment for medical frontliners.
S. Khan, et al. [21]	To predict the novel coronavirus transmission dynamics	Susceptible, Exposed, Infected, Recovered, Self-Quarantine, Isolation, Deceased	The different conditions of preparedness and response plan highlight the keys for outbreak downfall.
R. Cheng et al. [22]	To calculate the proportion of presymptomatic COVID-19 infections	Susceptible, Exposed, Presymptomatically Infectious, Symptomatically Infectious, Recovered	Proposed parametrization allows estimation of an initial susceptible proportion that is less than unity rather than assuming that the susceptible people comprise the country’s whole population, as is usually assumed.
L. Yang and T.L. Williams [23]	To analyze the patterns of COVID-19, to discuss potential anti-COVID-19 measures, and to explain why we need to conduct appropriate measures against COVID-19	Susceptible, Infected, Recovered	Anti-COVID-19 measures should include wearing a mask, washing one’s hands, keeping social distance, and staying at home if possible.
H.M. Youssef, et al. [24]	To predict the new COVID-19 model to be more suitable for more cases in any country by mathematical analysis of the considered model	Susceptible, Exposed, Infectious, Recovered	The ideal protocol consists of several steps and advice is introduced in detail to help the Saudi Arabia population to speed the breakdown spreading of COVID-19. One of the main subjects in that protocol is prevention is better than treatment.

Table 1. Cont.

Paper	Task	Compartments	Findings
P. Kumari, H.P. Singh, S. Singh [25]	To propose a model that includes the effect of quarantined cases, asymptomatic cases, and protected population to estimate the number of infected cases accurately	Susceptible, Exposed, Infected, Asymptomatic, Quarantined, Recovered, Dead, Insusceptible	In all the cases, simulation results show that the SEIAQRDT model fits the data better than the other models. The reason for this superiority is that the SEIAQRDT model describes suspected, infected with and without symptoms, recovered, quarantined, death, and exposed cases.
S. Gounana, et al. [26]	To model the spread of COVID-19 and investigate the impact of social distancing on the propagation of this pandemic	Susceptible, Infected, Recovered, Dead	Physical distancing or social distancing measures have an important effect on reducing the spread of COVID-19 by limiting face-to-face contact with others.
D. Mahayana, D.P. Natanael, M.F. Abbas [27]	To analyze and simulate several scenarios of the spread of a pandemic	Susceptible, Infected, Recovered, Dead	The SIR-D model has a higher performance value than the SIR model because the SIR-D model considers the separation between people who died and people who recovered.
M. Al-Raei, M.S. El-Daher, O. Solieva	To study the spreading and forecasting of the new coronavirus disease	Susceptible, Infected, Exposed, Recovered	The values of the SARS-CoV-2 basic reproduction number are reported to vary between 1.0158, returned for India, and 3.6642, returned for the United Kingdom, based on the simulation method used.

3. Materials and Methods

The proposed mathematical model for the spread of COVID-19 is presented as follows:

$$\begin{cases} \dot{V}_i = -\alpha_i V_i + (1 - \beta_i)(I_i + C_i) + \sum_{j=1, j \neq i}^n (1 - \alpha_j - G_{ij}) \varphi_{ij} \\ \dot{I}_i = \alpha_i V_i - \beta_i I_i + \gamma_i C_i + \sum_{j=1, j \neq i}^n (\alpha_j + G_{ij}) \varphi_{ij} \\ \dot{P}_i = \beta_i (I_i + C_i) \end{cases} \quad (1)$$

where

$i = 1 \dots n$;

V_i is the number of healthy residents of the i -th territorial sector;

I_i is the number of infected cases in the i -th territorial sector;

P_i is the number of fatal cases from COVID-19 in the i -th territorial sector;

N_i is the total number of infected people for the entire study period in the i -th territorial sector;

n_i is the total number of residents in the i -th territorial sector;

D is the total number of weeks of the study;

d_i is the total number of deaths from COVID-19 in the i -th territorial sector;

c_i is the total number of personnel (medical and support) involved in servicing infected patients in the i -th territorial sector;

C_i is the number of infected personnel (medical and support) who were involved in servicing infected patients in the i -th territorial sector;

φ_{ij} is passenger flow arriving in the sector i during the defined time interval (week) from the sector j ;

m_{ij} is the average number of flights from sector j to sector i during the defined time interval (week);

s_{ij} is the average area of vehicles used for transportation from sector j to sector i ; n is the number of sectors into which the study area is divided.

Auxiliary parameters $\alpha_i, \beta_i, \gamma_i, G_{ij}$, and S_{ij} are proposed to be calculated as follows:

$$\alpha_i = \frac{N_i}{n_i D} \tag{2}$$

$$\beta_i = \frac{d_i}{n_i D} \tag{3}$$

$$\gamma_i = \frac{C_i}{c_i D} \tag{4}$$

$$G_{ij} = \frac{1}{S_{ij} + \frac{1}{1-a_j}} \tag{5}$$

$$S_{ij} = \frac{m_{ij} s_{ij}}{\varphi_{ij}} \tag{6}$$

The generalized time interval for modeling is proposed to equal one week. Iterative calculations will be carried out according to each day to reduce the error inherent in weekly simulations. The peculiarities of the organization of the work of laboratory centers in the investigated territory, namely a day off on Sunday, leads to an uneven distribution of the number of PCR tests and confirmed cases by day. Based on the preceding, to assess the error of the proposed model, we chose the correspondence between the predicted and actual number of confirmed cases in one (calendar) week.

Based on the obtained initial data, described in detail in Section 5, the parameters of the mathematical model (1) acquired the following values:

$$V_1 = 3,176,404; I_1 = 244; P_1 = 7; N_1 = 445; n_1 = 3,176,648; D = 10; d_1 = 7 \tag{7}$$

Due to the complete absence at the time of the study of reliable information regarding the parameters $c_1, C_1, \varphi_{ij}, m_{ij}$, and s_{ij} , their values were taken to be equal to 0. Using (2)–(6), the initial values of other model parameters were calculated as following:

$$\alpha_1 = 0.000015; \beta_1 = 0.00000022; \gamma_1 = 0; G_{ij} = 0; S_{ij} = 0 \tag{8}$$

4. Results

In a sufficiently small neighborhood of the origin, the model has the classical topological structure of the phase portrait such as node, focus, saddle, etc. In the study of the bifurcations of systems, it is necessary to have a certain nomenclature of topological structures in R^3 .

When solving applied problems, it is precisely the degenerate states of the system that can qualitatively designate general dynamic tendencies in bifurcation states during catastrophes, collapses, and other restructurings.

The system of three linear differential equations of the third order can be represented as follows:

$$\begin{cases} \dot{x} = A_{11}x + A_{12}y + A_{13}z \\ \dot{y} = A_{21}x + A_{22}y + A_{23}z \\ \dot{z} = A_{31}x + A_{32}y + A_{33}z \end{cases} \tag{9}$$

In the non-degenerate case, linear system (9) has one equilibrium point $M(0; 0; 0)$ (the origin).

If the characteristic equation of system (9) has three real, unequal roots, then there is such a non-degenerate transformation

$$\begin{cases} \xi = c_{11}x + c_{12}y + c_{13}z \\ \eta = c_{21}x + c_{22}y + c_{23}z \\ \rho = c_{31}x + c_{32}y + c_{33}z \end{cases} \tag{10}$$

which brings system (9) to the form

$$\begin{cases} \dot{\xi} = \lambda_1 \xi \\ \dot{\eta} = \lambda_2 \eta \\ \dot{\rho} = \lambda_3 \rho \end{cases} \tag{11}$$

whose characteristic matrix will look like

$$G_1 = \begin{pmatrix} \lambda_1 & 0 & 0 \\ 0 & \lambda_2 & 0 \\ 0 & 0 & \lambda_3 \end{pmatrix} \tag{12}$$

Integrating (11), we obtain

$$\begin{cases} \xi = C_1 e^{\lambda_1 t} \\ \eta = C_2 e^{\lambda_2 t} \\ \rho = C_3 e^{\lambda_3 t} \end{cases} \tag{13}$$

For a qualitative analysis of the behavior of the phase trajectories of system (9) in the vicinity of the origin, we pass to the boundary:

$$\lambda_1 > 0, \text{ then } \lim_{t \rightarrow \infty} \xi(t) = \infty; \lambda_1 < 0, \text{ then } \lim_{t \rightarrow \infty} \xi(t) = 0 \tag{14}$$

$$\lambda_2 > 0, \text{ then } \lim_{t \rightarrow \infty} \eta(t) = \infty; \lambda_2 < 0, \text{ then } \lim_{t \rightarrow \infty} \eta(t) = 0 \tag{15}$$

$$\lambda_3 > 0, \text{ then } \lim_{t \rightarrow \infty} \rho(t) = \infty; \lambda_3 < 0, \text{ then } \lim_{t \rightarrow \infty} \rho(t) = 0 \tag{16}$$

When the discriminant of the characteristic equation of system (9) is equal to zero, one of the roots of the characteristic equation has a multiplicity of two and, in degenerate cases, three. In this case, the characteristic matrix of system (9) can have one of the following possible configurations:

$$G_2 = \begin{pmatrix} \lambda_1 & 0 & 0 \\ 0 & \lambda_1 & 0 \\ 0 & 0 & \lambda_3 \end{pmatrix} \tag{17}$$

$$G_3 = \begin{pmatrix} \lambda_1 & 0 & 0 \\ 0 & \lambda_1 & 0 \\ 0 & 0 & \lambda_1 \end{pmatrix} \tag{18}$$

$$G_4 = \begin{pmatrix} \lambda_1 & 1 & 0 \\ 0 & \lambda_1 & 0 \\ 0 & 0 & \lambda_2 \end{pmatrix} \tag{19}$$

$$G_5 = \begin{pmatrix} \lambda_1 & 1 & 0 \\ 0 & \lambda_1 & 1 \\ 0 & 0 & \lambda_1 \end{pmatrix} \tag{20}$$

In the case when the pair of eigenvalues λ_2 and λ_3 are complex, the matrix G_1 will take on a complex form.

$$\begin{pmatrix} \lambda_1 & 0 & 0 \\ 0 & \alpha + i\beta & 0 \\ 0 & 0 & \alpha - i\beta \end{pmatrix} \tag{21}$$

In order to bring the system to the simplest, real form, by means of a non-degenerate transformation, we perform the transition from η, ρ to U, V as follows:

$$\begin{cases} \xi = \xi \\ \eta = U + iV \\ \rho = U - iV \end{cases} \tag{22}$$

From here we obtain the following:

$$\begin{cases} U = (\eta + \rho)/2 \\ V = (\eta - \rho)/2i \end{cases} \tag{23}$$

From (23), using (11), we obtain

$$\dot{U} = \frac{\dot{\eta} + \dot{\rho}}{2} = \frac{\lambda_2\eta + \lambda_3\rho}{2} = \frac{(\alpha + i\beta)(u + iV) + (\alpha - i\beta)(u - iV)}{2} = \alpha U + \beta V \tag{24}$$

Similarly,

$$\dot{V} = \alpha V - \beta U \tag{25}$$

Therefore, under the condition that in system (11) λ_2 and λ_3 are complex conjugate, there is such a non-degenerate transformation that reduces system (22) to the form

$$\begin{cases} \dot{\xi} = \lambda_1\xi \\ \dot{U} = \alpha U + \beta V \\ \dot{V} = -\beta U + \alpha V \end{cases} \tag{26}$$

The characteristic matrix of such a system will look like

$$G_6 = \begin{pmatrix} \lambda_1 & 0 & 0 \\ 0 & \alpha & \beta \\ 0 & -\beta & \alpha \end{pmatrix} \tag{27}$$

Let us make the transition to a cylindrical coordinate system:

$$\begin{cases} \xi = \xi \\ U = r\cos\theta \\ V = r\sin\theta \end{cases} \tag{28}$$

By transformations, using the equality $U^2 + V^2 = r^2$, we obtain $\dot{r} = \alpha r$, and according to system (28) we obtain $t\dot{g}\theta = V/U$. Differentiating the resulting trigonometric equation and using (26) and (28), we obtain the following:

$$\begin{cases} \xi = C_1 e^{\lambda_1 t} \\ r = r_0 e^{\alpha t} \\ \theta = \beta t + \theta_0 \end{cases} \tag{29}$$

Let us move on to the border:

$$\alpha > 0, \text{ then } \lim_{t \rightarrow \infty} r(t) = \infty; \alpha < 0, \text{ then } \lim_{t \rightarrow \infty} r(t) = 0 \tag{30}$$

$$\beta > 0, \text{ then } \lim_{t \rightarrow \infty} \theta(t) = \infty; \beta < 0, \text{ then } \lim_{t \rightarrow \infty} \theta(t) = -\infty \tag{31}$$

$$\alpha = 0, \text{ then } \lim_{t \rightarrow \infty} r(t) = \text{const} \tag{32}$$

In the case when two of the three roots of the characteristic equation are completely imaginary, but $Det(J) \neq 0$, the characteristic matrix of system (9) takes the form

$$G_1 = \begin{pmatrix} \lambda_1 & 0 & 0 \\ 0 & 0 & \beta \\ 0 & -\beta & 0 \end{pmatrix} \tag{33}$$

Figure 1 schematically shows the phase portraits of system (9) with characteristic matrices (G_1 – G_7).

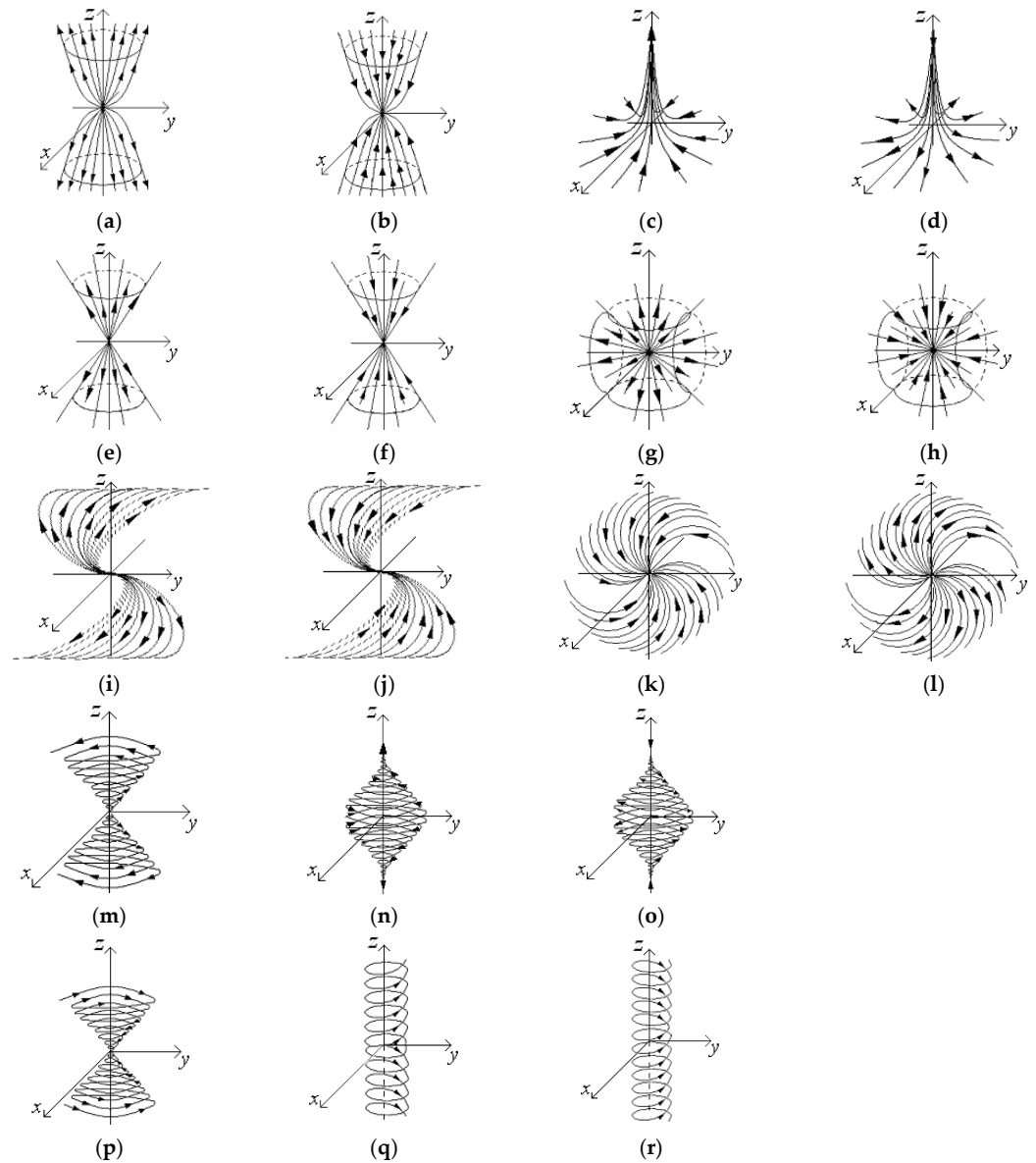


Figure 1. Schematic representation of the topology of the phase space of system (9) in the vicinity of a singular point: (a)—triaxial unstable node; (b)—triaxial stable assembly; (c)—stable saddle; (d)—unstable saddle; (e)—unstable two-phase-star node; (f)—stable two-phase-star node; (g)—unstable three-phase-star node; (h)—stable three-phase-star node; (i)—unstable two-phase degenerate node; (j)—stable two-phase degenerate node; (k)—unstable three-phase degenerate node; (l)—stable three-phase degenerate node; (m)—divergent unstable focus; (n)—mismatched stable focus; (o)—convergent unstable focus; (p)—coinciding stable focus; (q)—divergent center; (r)—coinciding center.

If all eigenvalues of the characteristic matrix of system (9) are real, have the same sign, and are not equal to each other, the projections of phase trajectories onto all three planes form a classical stable or unstable node. The singular point of the origin of system (9) has real eigenvalues of the characteristic matrix and saddle provided that at least one pair of eigenvalues of the characteristic matrix of system (9) has opposite signs. The projection of phase trajectories onto one of the planes forms a stable (Figure 1c) and unstable (Figure 1d) node. And when projected onto the other two planes, a saddle appears. The cases of hyperbolic points shown in Figure 1e–l are characterized by the multiplicity of the roots of the characteristic equation and are a special case of the “triaxial knot”. In the cases shown in Figure 1e,f,i,j, one of the roots of the characteristic equation has a multiplicity of two. For the cases presented in Figure 1e,f,i,j, the characteristic equation has a root of multiplicity three. When a pair of eigenvalues of the characteristic matrix is complex conjugate, then, when projected onto a plane xOy , the phase trajectories form a stable focus (Figure 1n,p), an unstable focus (Figure 1m,o), and a center (Figure 1q,r).

Table 2 shows the classification system of non-degenerate types of equilibrium points with their corresponding analytical conditions of occurrence and names.

Table 2. Types of simple system equilibrium points.

Figure	Characteristic Matrix	The Name of the Singular Point	Additional Terms
1a	G_1	Triaxial unstable node	$\lambda_1 > \lambda_2 > \lambda_3 > 0$
1b	G_1	Triaxial stable node	$\lambda_1 < \lambda_2 < \lambda_3 < 0$
1c	G_1	Stable saddle	$\lambda_1 < \lambda_2 < 0, \lambda_3 > 0$
1d	G_1	Unstable saddle	$\lambda_1 > \lambda_2 > 0, \lambda_3 < 0$
1e	G_2	Unstable two-phase-star node	$\lambda_1 > \lambda_2 > 0$
1f	G_2	Stable two-phase-star-node	$\lambda_1 < \lambda_2 < 0$
1g	G_3	Unstable three-phase-star node	$\lambda_1 > 0$
1h	G_3	Stable three-phase-star node	$\lambda_1 < 0$
1i	G_4	Unstable two-phase degenerate node	$\lambda_1 > \lambda_2 > 0$
1j	G_4	Stable two-phase degenerate node	$\lambda_1 < \lambda_2 < 0$
1k	G_5	Unstable three-phase degenerate node	$\lambda_1 > 0$
1l	G_5	Stable three-phase degenerate node	$\lambda_1 < 0$
1m	G_6	Divergent unstable focus	$\lambda_3 > 0, \alpha > 0$
1n	G_6	Divergent steady focus	$\lambda_3 > 0, \alpha < 0$
1o	G_6	Compatible unstable focus	$\lambda_3 < 0, \alpha > 0$
1p	G_6	Compatible stable focus	$\lambda_3 < 0, \alpha < 0$
1q	G_7	Divergent center	$\lambda_1 > 0$
1r	G_7	Compatible center	$\lambda_1 < 0$

In Table 2 and below, the following notation will be used: $\lambda_1, \lambda_2,$ and λ_3 are real eigenvalues of the characteristic matrix of the system at the equilibrium point M ; α is a real part of a pair of complex conjugate eigenvalues of the characteristic matrix of system (9).

Together with simple types of equilibrium points, a number of folded equilibrium points of covariance n are possible, that is, those whose occurrence is due to the fact that the real part n of the roots of the characteristic equation is equal to zero. It is well known that the simplest form of the characteristic matrix of system (9), which has a complex equilibrium point of codimensionality 1 in the vicinity of the origin, can only be represented in the following way:

$$G_8 = \begin{pmatrix} \lambda_1 & 0 & 0 \\ 0 & 0 & 0 \\ 0 & 0 & \lambda_2 \end{pmatrix} \tag{34}$$

$$G_9 = \begin{pmatrix} \lambda_1 & 0 & 0 \\ 0 & 0 & 0 \\ 0 & 0 & \lambda_1 \end{pmatrix} \tag{35}$$

$$G_{10} = \begin{pmatrix} \lambda_1 & 0 & 1 \\ 0 & 0 & 0 \\ 0 & 0 & \lambda_1 \end{pmatrix} \tag{36}$$

$$G_{11} = \begin{pmatrix} \alpha & \beta & 0 \\ -\beta & \alpha & 0 \\ 0 & 0 & 0 \end{pmatrix} \tag{37}$$

$$G_{12} = \begin{pmatrix} 0 & \beta & 0 \\ -\beta & 0 & 0 \\ 0 & 0 & 0 \end{pmatrix} \tag{38}$$

Figure 2 shows a schematic representation of the topology of the phase space of system (9) in the vicinity of the composed singular point.

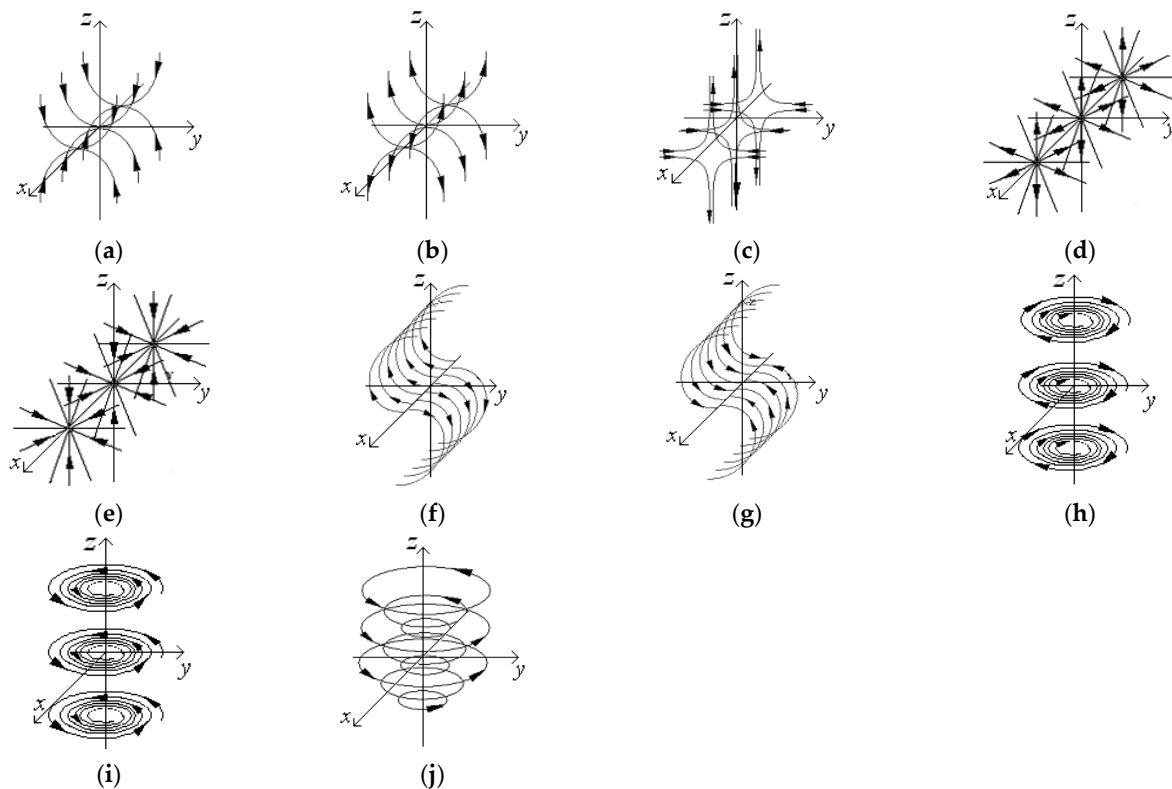


Figure 2. Schematic representation of the topology of the phase space of system (9) in the vicinity of the composed singular point: (a)—single-phase degenerate stable node; (b)—single-phase degenerate unstable node; (c)—degenerate saddle; (d)—an unstable degenerate stellar node; (e)—stable degenerate star node; (f)—unstable congenital cylinder; (g)—stable congenital cylinder; (h)—congenital unstable focus; (i)—congenital stable focus; (j)—congenital center.

The phase portraits presented in Figure 2 are characterized by the presence of one zero root of the characteristic equation. When projecting phase portraits onto planes corresponding to non-zero real roots or pairs of complex roots of the characteristic equation, a stable node (Figure 2a), an unstable node (Figure 2b), a saddle (Figure 2c), an unstable star node (Figure 2d), stable stellar node (Figure 2e), unstable degenerate node (Figure 2f), stable degenerate node (Figure 2g), unstable focus (Figure 2h), stable focus (Figure 2i), and center (Figure 2j), respectively, are formed.

The classification of folded equilibrium points of codimension 1 is given in Table 3.

Table 3. Types of stacked equilibrium points of codimension 1 of system (9).

Figure	Characteristic Matrix	The Name of the Singular Point	Additional Terms
2a	G_8	Single-phase degenerate stable node	$\lambda_1 < \lambda_2 < 0$
2b	G_8	Single-phase degenerate unstable node	$\lambda_1 > \lambda_2 > 0$
2c	G_8	Degenerate saddle	$\lambda_1 \lambda_2 < 0$
2d	G_9	Unstable degenerate star node	$\lambda_1 > 0$
2e	G_9	Stable degenerate star node	$\lambda_1 < 0$
2f	G_{10}	Unstable degenerate cylinder	$\lambda_1 > 0$
2g	G_{10}	Stable degenerate cylinder	$\lambda_1 < 0$
2h	G_{11}	Degenerate unstable focus	$\alpha > 0$
2i	G_{11}	Degenerate persistent focus	$\alpha < 0$
2j	G_{12}	Degenerate center	$\alpha = 0$

The characteristic matrix of system (9), which has a complex equilibrium point of codimension 2 in the vicinity of the origin, can only be reduced to the form:

$$G_{13} = \begin{pmatrix} 0 & 0 & 0 \\ 0 & 0 & 0 \\ 0 & 0 & \lambda_1 \end{pmatrix} \tag{39}$$

Figure 3 shows a schematic representation of the topology of the phase space of system (9) in the vicinity of the composed singular point of codimension 2.



Figure 3. Schematic representation of the topology of the phase space of system (9) in the vicinity of the composed singular point of codimension 2: (a)—“unstable stationary plane”, (b)—“stable stationary plane”.

The phase space of system (9) (Figure 3a,b) contains an infinite number of equilibrium points placed infinitely close to each other, forming a stationary surface (in the case of a linear system, a plane); phase trajectories either approach (attractor) or move away from it (repeller). Based on the considerations outlined above, we consider it appropriate to use the names “unstable stationary plane” and “stable stationary plane” for such points, respectively.

The types of folded equilibrium points of codimension 2 of the system are presented in Table 4.

Table 4. Types of folded equilibrium points of codimension 2 of system (9).

Figure	Characteristic Matrix	The Name of the Singular Point	Additional Terms
2a	G_{13}	Unstable stationary plane	$\lambda_1 > 0$
2b	G_{13}	Stable stationary plane	$\lambda_1 < 0$

In addition to the equilibrium points of system (9) presented above, a case may arise when the system is stationary in all states: “stationary space”. The characteristic matrix of system (9) corresponding to such a state will be zero, and the phase portrait will contain only stationary points (Figure 4).

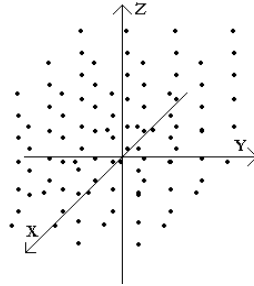


Figure 4. Phase portrait of system (9) in case of zero characteristic matrix.

The names of topological structures in the proposed classification are formed similarly to the two-dimensional case.

5. Case Studies

5.1. Dnipropetrovsk Region (Ukraine)

The object of the study is the human population of the Dnipropetrovsk region (Ukraine) and the process of the spread of the COVID-19 infection in it.

The Dnipropetrovsk region is a region in Ukraine located in the country’s central, eastern, and southern parts. The area of the region is 31.9 thousand km². The population is 3,300,309 people (as of 1 June 2013, 7.3% of the state’s population lives here). The center of the region and the largest city is Dnipro.

It should be emphasized that there are no reliable data on the source of infection, “zero patient,” concomitant diseases, etc. Statistical data collected on the infected are usually not representative. Actuality, completeness, reliability, and other statistical information characteristics are unreliable. The data used for the case study were collected before the full-scale Russian invasion of Ukraine, which led to the mass migration of Ukrainian citizens.

However, the large area and population of the investigated territory make the obtained results reliable for application to other world territories.

The study was based on the understanding of the population as a set of individuals, which can be conditionally divided into the following groups:

- Healthy (uninfected) population;
- Infected patients;
- Patients who dropped out of the study (dead or recovered);
- Patients living in specific territorial sectors;
- Men and women;
- Age group (up to 15 years old, from 15 to 55 years old, over 55 years old);
- Medical and support staff involved in the care of the infected.

At the time of the study, it is generally accepted that re-infection of a person is unlikely. The fact that an infected patient receives immunity after recovery has not been confirmed. However, at the same time, world incidence statistics show that examples of re-infection are either absent or relatively rare, which, in turn, may be due to incomplete treatment and false negative test results at the time of discharge from the hospital.

Table 5 shows the factors taken into account in the mathematical model and the sources from which the information was obtained.

Table 5. Data characteristics.

Factors	Information Source
Territorial division of the Dnipropetrovsk region	Main Department of Statistics in Dnipropetrovsk region
Gender and age structure of the population	Main Department of Statistics in Dnipropetrovsk region
Gender and age structure of those infected	Dnipropetrovsk Regional Laboratory Center
The factor of the absence of quarantine restrictions	Dnipropetrovsk Regional State Administration
Number of suspected, infected, dead, and recovered by day	Dnipropetrovsk Regional Laboratory Center
Statistical data on the course of the COVID-19 epidemic in other countries	Open sources
Features of the course of the disease	Expert opinion

The results of the numerical experiment conducted from 22 July 2021 till 15 September 2021, for a period of 56 days (8 weeks), are presented in Table 6.

Table 6. Mathematical forecast of the number of confirmed cases of infection in the population of the Dnipropetrovsk region (for the period from 22 July 2021 to 15 September 2021).

Date	Realistic Forecast	Optimistic Forecast	Pessimistic Forecast	Date	Realistic Forecast	Optimistic Forecast	Pessimistic Forecast
22 July 2021	13	10	22	19 August 2021	23	18	32
23 July 2021	14	11	23	20 August 2021	24	19	34
24 July 2021	15	12	25	21 August 2021	24	19	34
25 July 2021	15	12	25	22 August 2021	27	22	38
26 July 2021	15	12	25	23 August 2021	31	25	43
27 July 2021	15	12	26	24 August 2021	33	26	46
28 July 2021	17	14	29	25 August 2021	34	27	48
29 July 2021	16	13	28	26 August 2021	36	29	50
30 July 2021	19	15	33	27 August 2021	38	30	53
31 July 2021	21	16	35	28 August 2021	39	31	55
1 August 2021	17	14	30	29 August 2021	41	33	57
2 August 2021	18	14	30	30 August 2021	43	34	60
3 August 2021	18	14	30	31 August 2021	45	36	63
4 August 2021	18	14	31	1 September 2021	48	38	67
5 August 2021	18	15	31	2 September 2021	52	42	73
6 August 2021	19	15	32	3 September 2021	55	44	77
7 August 2021	19	15	33	4 September 2021	56	45	78
8 August 2021	20	16	34	5 September 2021	57	46	80
9 August 2021	20	16	35	6 September 2021	64	51	90
10 August 2021	20	16	35	7 September 2021	66	53	92
11 August 2021	20	16	35	8 September 2021	67	54	94
12 August 2021	20	16	36	9 September 2021	71	57	99
13 August 2021	21	17	37	10 September 2021	77	62	108
14 August 2021	21	17	37	11 September 2021	80	64	112
15 August 2021	21	17	38	12 September 2021	82	66	115
16 August 2021	22	17	30	13 September 2021	86	69	120
17 August 2021	22	18	30	14 September 2021	101	81	141
18 August 2021	22	18	31	15 September 2021	106	85	148

According to the results of the numerical calculation, fourteen forecasts were made (dated 22 July, 29 July, 5 August, 12 August, 19 August, 26 August, 2 September, 9 September, 16 September, 24 September, 21 October, 20 November, and 29 December). Each of the forecasts was built for a period of 90 days. Table 7 provides information on the modeling error for each of the fourteen predictions.

Table 7. Analysis of the error of developed forecasts of the dynamics of COVID-19 in the Dnipropetrovsk region.

Date of Forecast	Duration of Forecast	Error
22 July 2021	1 week	0.0%
29 July 2021	1 week	5.45%
5 August 2021	1 week	8.6%
12 August 2021	1 week	7.0%
19 August 2021	1 month	3.8%
26 August 2021	1 week	3.1%
2 September 2021	1 week	1.6%
9 September 2021	1 week	4.12%
16 September 2021	1 month	8.4%
24 September 2021	1 month	17.0%
21 October 2021	1 month	9.8%
20 November 2021	1 month	11.5%
29 December 2021	3 month	13.1%
29 December 2021	6 month	19.6%

5.2. Kharkiv Region (Ukraine)

The object of the study is the human population of the Kharkiv region (Ukraine) and the process of the spread of the COVID-19 infection in it.

The Kharkiv region is a region in Ukraine located in the country’s central, eastern, and southern parts. The area of the region is 31.415 thousand km². The population is 2,633,834 people (as of 1 June 2013, 7.3% of the state’s population lives here). The center of the region and the largest city is Kharkiv.

We used the same assumptions and population groups as in previous case study.

Table 8 shows the factors taken into account in the mathematical model and the sources from which the information was obtained.

Table 8. Data characteristics.

Factors	Information Source
Territorial division of the Kharkiv region	Main Department of Statistics in Kharkiv region
Gender and age structure of the population	Main Department of Statistics in Kharkiv region
Gender and age structure of those infected	Kharkiv Regional Laboratory Center
The factor of the absence of quarantine restrictions	Kharkiv Regional State Administration
Number of suspected, infected, dead, and recovered by day	Kharkiv Regional Laboratory Center
Statistical data on the course of the COVID-19 epidemic in other countries	Open sources
Features of the course of the disease	Expert opinion

The results of the numerical experiment conducted from 27 March 2023 till 21 May 2023, for a period of 56 days (8 weeks), are presented in the Table 9.

Table 9. Mathematical forecast of the number of confirmed cases of infection in the population of the Kharkiv region (for the period from 27 March 2023 to 21 May 2023).

Date	Realistic Forecast	Optimistic Forecast	Pessimistic Forecast	Date	Realistic Forecast	Optimistic Forecast	Pessimistic Forecast
27 March 2023	7	5	9	24 April 2023	12	15	21
28 March 2023	2	5	9	25 April 2023	14	18	25
29 March 2023	6	5	9	26 April 2023	17	21	29

Table 9. Cont.

Date	Realistic Forecast	Optimistic Forecast	Pessimistic Forecast	Date	Realistic Forecast	Optimistic Forecast	Pessimistic Forecast
30 March 2023	5	6	10	27 April 2023	18	23	32
31 March 2023	3	6	10	28 April 2023	19	24	34
1 April 2023	5	6	10	29 April 2023	22	28	39
2 April 2023	7	6	10	30 April 2023	25	31	43
3 April 2023	11	7	11	1 May 2023	29	36	50
4 April 2023	6	7	11	2 May 2023	26	32	45
5 April 2023	4	7	11	3 May 2023	25	31	43
6 April 2023	5	7	11	4 May 2023	24	30	42
7 April 2023	4	8	12	5 May 2023	29	36	50
8 April 2023	9	8	12	6 May 2023	27	34	48
9 April 2023	7	8	12	7 May 2023	26	33	46
10 April 2023	9	8	12	8 May 2023	27	34	48
11 April 2023	13	8	12	9 May 2023	30	38	53
12 April 2023	15	9	13	10 May 2023	32	40	56
13 April 2023	3	10	14	11 May 2023	34	42	59
14 April 2023	5	10	14	12 May 2023	37	46	64
15 April 2023	6	10	14	13 May 2023	35	44	62
16 April 2023	3	10	14	14 May 2023	32	40	56
17 April 2023	9	10	14	15 May 2023	31	39	55
18 April 2023	4	11	15	16 May 2023	30	37	52
19 April 2023	11	11	15	17 May 2023	28	35	49
20 April 2023	12	12	16	18 May 2023	30	38	53
21 April 2023	4	12	16	19 May 2023	33	41	57
22 April 2023	8	12	16	20 May 2023	34	43	60
23 April 2023	3	13	17	21 May 2023	36	45	63

According to the results of the numerical calculation, fourteen forecasts were made (dated 27 March, 3 April, 10 April, 17 April, 24 April, 1 May, 8 May, 15 May, 2 June, 4 July, 1 August, and 2 September). Each of the forecasts was built for a period of 92 days. The Table 10 provides information on the modeling error for each of the fourteen predictions.

Table 10. Analysis of the error of developed forecasts of the dynamics of COVID-19 in Kharkiv region.

Date of Forecast	Duration of Forecast	Error
27 March 2023	1 week	12.30%
4 April 2023	1 week	14.45%
10 April 2023	1 week	11.31%
17 April 2023	1 week	16.03%
24 April 2023	1 week	10.12%
1 May 2023	1 week	12.63%
8 May 2023	1 week	17.30%
15 May 2023	1 week	9.43%
1 May 2021	1 month	21.60%
2 June 2021	1 month	26.08%
4 July 2021	1 month	22.44%
1 August 2021	1 month	14.21%
2 August 2021	3 month	26.82%
2 September 2021	6 month	28.00%

6. Conclusions

In this paper, a novel mathematical model has been successfully developed to forecast the spread of both COVID-19 and similar infectious diseases using a system of autonomous differential equations. The model parameters are easily configured based on data provided from the official repositories. The adequacy of the model was confirmed by testing on the example of the spread of COVID-19 in one of the largest regions of Ukraine, both in

terms of population and area. As a result of the development of the model, six 90-day forecasts of the infected population were generated, each of which demonstrated a high level of accuracy with an error of no more than 3.8%. The results of these forecasts and the numerical experiment contributed to the development of sound recommendations for the health authorities of the region on the implementation of the quarantine period. This work contributes to understanding the dynamics of the spread of COVID-19 and similar infections, which provides support for decision making by public health authorities.

The main added values of our model lie in its unique approach to forecasting the spread of infectious diseases and its adaptability to various real-world contexts. The model not only provides high accuracy in predictions but also offers a flexible framework that can be customized for different regions and population demographics. This adaptability makes it a valuable tool for public health authorities to effectively develop targeted strategies to manage infectious disease outbreaks. The model's integration of multiple parameters and its capacity for bifurcation analysis enhance its utility in identifying critical factors that influence the spread of infections, thus enabling proactive and informed decision making.

A critical aspect of our model is the assumptions regarding population homogeneity and data quality. While necessary for the initial development and testing of the model, these assumptions present limitations when applied to regions with significant demographic or behavioral variations. Data quality is paramount to the model's accuracy; hence, ensuring reliable data collection methods is crucial. When high-quality data is unavailable, the model's performance may be affected. However, we have used official data on COVID-19 morbidity for our study.

Another area that requires further exploration is the model's adaptability to different regions and public health scenarios. The necessity for highly reliable and precise data poses a significant challenge, particularly in less developed regions or during the early stages of an outbreak when data may be scarce or inconsistent. Investigating the model's performance under varying data quality conditions and developing strategies to mitigate these issues will be essential. Potential solutions include using data augmentation techniques, cross-validation with alternative data sources, and continuously incorporating real-time data feeds to refine model predictions.

Further research should explore the model's applicability in public health emergencies beyond COVID-19. We can better understand its versatility and limitations by testing the model with different infectious diseases and varying public health interventions. Integrating additional data sources, such as mobility patterns, social media trends, and environmental factors, could enhance the model's predictive power and responsiveness. This would enable public health authorities to deploy the model in various scenarios, providing a robust tool for managing current and future public health emergencies.

The study of the bifurcation properties of the presented mathematical model made it possible to establish 18 non-degenerate states of the system, 10 degenerate states of codimension 1, and two degenerate states of codimension 2. Analytical conditions for the occurrence of bifurcations determine the system parameters under which such transitions can occur. An interesting fact is that almost all topologies, except for diacritical degenerate nodes, have a fairly clear applied interpretation. This substantiates the adequacy of such models in relation to systems and processes of various natures. The proposed models can be used for systems with a large number of parameters and influence factors.

From the applied point of view, it is not the bifurcations themselves that are interesting, but non-degenerate states that can be changed by passing through the bifurcation value of the defining parameter. It should be noted that not all non-degenerate states are compatible with each other. The applied interpretation of non-degenerate system states also proves that not all of them can be transformed by trivial changes. The situation when several invariants change sign in the system is characterized by a bifurcation of higher orders. When a bifurcation of codimension equal to the dimension of the system arises, any changes in the topology are possible. At the same time, it is obvious that such a bifurcation point is actually a point of complete rest, at which all the defining parameters of the model

change. However, from an applied point of view, such a bifurcation is of little interest. It was established in the work that the state of the system with a hyperbolic equilibrium point is not typical for the presented applied problem. Hyperbolic systems are typical for problems of mathematical economics, biology, psychology, etc. For problems of the spread of infectious diseases, systems with elliptical equilibrium points are usually applicable. The reason for this may be the stability of the system and its isolation, as well as the existence of pronounced intrasystem dynamics (homomorphism).

The scientific novelty of the work lies in the development of a new mathematical model of the dynamics of infectious diseases, approaches to the qualitative study of such a model, analysis of the analytical conditions of qualitative changes in the system (bifurcations), and approaches to the applied interpretation of the results obtained, which allows evaluating not only the qualitative modes of operation but also the methods and results of the management system.

The practical novelty of the work lies in the possibility of applying the proposed approaches and mathematical models to predict the dynamics of the spread of infectious disease, using the example of COVID-19. Retrospective analysis showed the high accuracy of the model and the adequacy of its management recommendations. It allows not only an up-to-date forecast of the system's state to be obtained but also recommendations for its management to change the quality modes of operation to be developed.

Author Contributions: Conceptualization, O.K. (Olena Kiseleva) and S.Y.; methodology, O.K. (Olena Kiseleva), S.Y. and O.K. (Oleksandr Kuzenkov); software, O.K. (Oleksandr Kuzenkov) and D.C.; validation, D.C. and O.K. (Oleksandr Kuzenkov); formal analysis, D.C. and S.Y.; investigation, O.K. (Olena Kiseleva), D.C. and O.K. (Oleksandr Kuzenkov); resources, D.C.; data curation, O.K. (Olena Kiseleva) and O.K. (Oleksandr Kuzenkov); writing—original draft preparation, D.C. and O.K. (Oleksandr Kuzenkov); writing—review and editing, O.K. (Olena Kiseleva) and S.Y.; visualization, O.K. (Oleksandr Kuzenkov); supervision, O.K. (Olena Kiseleva) and S.Y.; project administration, D.C.; funding acquisition, D.C. All authors have read and agreed to the published version of the manuscript.

Funding: The research is funded by National Science Center under the IMPRESS-U program within the framework of the project 2023/05/Y/ST6/00263 entitled "Modeling and forecasting the spread of infection in war and post-war period using epidemiological, behavioral and genomic surveillance data".

Data Availability Statement: The data presented in this study are available upon request from the corresponding author.

Conflicts of Interest: The authors declare no conflicts of interest.

References

1. Cucinotta, D.; Vanelli, M. WHO Declares COVID-19 a Pandemic. *Acta Bio-Medica Atenei Parm.* **2020**, *91*, 157–160. [CrossRef]
2. Bestetti, R.B.; Furlan-Daniel, R.; Couto, L.B. Nonpharmaceutical Public Health Interventions to Curb the COVID-19 Pandemic: A Narrative Review. *J. Infect. Dev. Ctries.* **2022**, *16*, 583–591. [CrossRef] [PubMed]
3. Saleem, F.; AL-Ghamdi, A.S.A.-M.; Alassafi, M.O.; AlGhamdi, S.A. Machine Learning, Deep Learning, and Mathematical Models to Analyze Forecasting and Epidemiology of COVID-19: A Systematic Literature Review. *Int. J. Environ. Res. Public Health* **2022**, *19*, 5099. [CrossRef] [PubMed]
4. Spinella, C.; Mio, A.M. Simulation of the Impact of People Mobility, Vaccination Rate, and Virus Variants on the Evolution of COVID-19 Outbreak in Italy. *Sci. Rep.* **2021**, *11*, 23225. [CrossRef]
5. Wang, P.; Zheng, X.; Liu, H. Simulation and Forecasting Models of COVID-19 Taking into Account Spatio-Temporal Dynamic Characteristics: A Review. *Front. Public Health* **2022**, *10*, 1033432. [CrossRef]
6. Bosa, I.; Castelli, A.; Castelli, M.; Ciani, O.; Compagni, A.; Galizzi, M.M.; Garofano, M.; Ghislandi, S.; Giannoni, M.; Marini, G.; et al. Response to COVID-19: Was Italy (Un)Prepared? *Health Econ. Policy Law* **2021**, *17*, 1–13. [CrossRef]
7. Bernasconi, A.; Canakoglu, A.; Masseroli, M.; Pinoli, P.; Ceri, S. A Review on Viral Data Sources and Search Systems for Perspective Mitigation of COVID-19. *Brief. Bioinform.* **2021**, *22*, 664–675. [CrossRef]
8. Kong, L.; Duan, M.; Shi, J.; Hong, J.; Chang, Z.; Zhang, Z. Compartmental Structures Used in Modeling COVID-19: A Scoping Review. *Infect. Dis. Poverty* **2022**, *11*, 72. [CrossRef]
9. Ross, R. The logical basis of the sanitary policy of mosquito reduction. *Science* **1905**, *22*, 689–699. [CrossRef]
10. Ross, R. Report on the Prevention of Malaria in Mauritius. Available online: <https://wellcomecollection.org/works/rjj6m9qm> (accessed on 29 May 2023).

11. L., W.B. The Prevention of Malaria. *Nature* **1910**, *85*, 263–264. [[CrossRef](#)]
12. Macdonald, G. The Measurement of Malaria Transmission. *Proc. R. Soc. Med.* **1955**, *48*, 295–302. [[CrossRef](#)] [[PubMed](#)]
13. Hoppensteadt, F. An Age Dependent Epidemic Model. *J. Frankl. Inst.* **1974**, *297*, 325–333. [[CrossRef](#)]
14. Hoppensteadt, F. *Mathematical Theories of Populations: Demographics, Genetics, and Epidemics*; Society of Industrial and Applied Mathematics: Philadelphia, PA, USA, 1975; pp. i–ix.
15. Li, X.-Z.; Gupur, G.; Zhu, G.-T. Threshold and Stability Results for an Age-Structured SEIR Epidemic Model. *Comput. Math. Appl.* **2001**, *42*, 883–907. [[CrossRef](#)]
16. Inaba, H. Threshold and Stability Results for an Age-Structured Epidemic Model. *J. Math. Biol.* **1990**, *28*, 411–434. [[CrossRef](#)] [[PubMed](#)]
17. Park, T. *Age-Dependence in Epidemic Models of Vector-Borne Infections*; The University of Alabama: Tuscaloosa, AL, USA, 2004.
18. Shin, H.-Y. A Multi-Stage SEIR(D) Model of the COVID-19 Epidemic in Korea. *Ann. Med.* **2021**, *53*, 1159–1169. [[CrossRef](#)] [[PubMed](#)]
19. Reno, C.; Lenzi, J.; Navarra, A.; Barelli, E.; Gori, D.; Lanza, A.; Valentini, R.; Tang, B.; Fantini, M.P. Forecasting COVID-19-Associated Hospitalizations under Different Levels of Social Distancing in Lombardy and Emilia-Romagna, Northern Italy: Results from an Extended SEIR Compartmental Model. *J. Clin. Med.* **2020**, *9*, 1492. [[CrossRef](#)]
20. Bhalraj, A.; Azmi, A. Modelling the Significant Effect of Public Health Interventions on COVID-19 Transmission. In *Analysis of Infectious Disease Problems (COVID-19) and Their Global Impact*; Infosys Science Foundation Series; Springer: Singapore, 2021; pp. 483–506. [[CrossRef](#)]
21. Khan, S.; Khan, M.W.; Kumar, N.; Dohare, R.; Sankhwar, S. Transmission Dynamics of COVID-19 Outbreak in India and Effectiveness of Self-Quarantine: A Phase-Wise Data Driven Analysis. *Int. J. Comput. Appl. Technol.* **2021**, *66*, 389–400. [[CrossRef](#)]
22. Cheng, R.; Dye, C.; Dagpunar, J.; Williams, B. Modelling Presymptomatic Infectiousness in COVID-19. *J. Symulation* **2023**, *17*, 532–543. [[CrossRef](#)]
23. Lu, Y.; Williams, T.L. Modeling Analytics in COVID-19: Prediction, Prevention, Control, and Evaluation. *J. Manag. Anal.* **2021**, *8*, 424–442. [[CrossRef](#)]
24. Youssef, H.M.; Alghamdi, N.A.; Ezzat, M.A.; El-Bary, A.A.; Shawky, A.M. A New Dynamical Modeling SEIR with Global Analysis Applied to the Real Data of Spreading COVID-19 in Saudi Arabia. *Math. Biosci. Eng.* **2020**, *17*, 7018–7044. [[CrossRef](#)]
25. Kumari, P.; Singh, H.P.; Singh, S. SEIAQRDT Model for the Spread of Novel Coronavirus (COVID-19): A Case Study in India. *Appl. Intell.* **2020**, *51*, 2818–2837. [[CrossRef](#)] [[PubMed](#)]
26. Gounane, S.; Barkouch, Y.; Atlas, A.; Bendahmane, M.; Karami, F.; Meskine, D. An Adaptive Social Distancing SIR Model for COVID-19 Disease Spreading and Forecasting. *Epidemiol. Methods* **2021**, *10*, 20200044. [[CrossRef](#)]
27. Mahayana, D.; Petra Natanael, D.; Fadhl ‘Abbas, M. Analysis and Simulation of COVID-19 Spread in Indonesia Using SIR and SIR-D Modelling with Optimization. *Int. J. Electr. Eng. Inform.* **2022**, *14*, 344–357. [[CrossRef](#)]
28. Al-Raei, M.; El-Daher, M.S.; Solieva, O. Applying SEIR Model without Vaccination for COVID-19 in Case of the United States, Russia, the United Kingdom, Brazil, France, and India. *Epidemiol. Methods* **2021**, *10*, 20200036. [[CrossRef](#)]

Disclaimer/Publisher’s Note: The statements, opinions and data contained in all publications are solely those of the individual author(s) and contributor(s) and not of MDPI and/or the editor(s). MDPI and/or the editor(s) disclaim responsibility for any injury to people or property resulting from any ideas, methods, instructions or products referred to in the content.